Structural Elements Involved in Proton Translocation by Cytochrome *c* Oxidase as Revealed by Backbone Amide Hydrogen−Deuterium Exchange of the E286H Mutant†

Laura S. Busenlehner,‡,# Gisela Brändén,§ Ida Namslauer,§ Peter Brzezinski,*,§ and Richard N. Armstrong*,‡

Departments of Biochemistry and Chemistry, Center in Molecular Toxicology, Vanderbilt University, Nashville, Tennessee 37232-0146, and Department of Biochemistry and Biophysics, The Arrhenius Laboratories for Natural Sciences, Stockholm University, Stockholm, SE-106 91, Sweden

Received August 14, 2007; Revised Manuscript Received October 17, 2007

ABSTRACT: Cytochrome *c* oxidase is the terminal electron acceptor in the respiratory chains of aerobic organisms and energetically couples the reduction of oxygen to water to proton pumping across the membrane. The mechanisms of proton uptake, gating, and pumping have yet to be completely elucidated at the molecular level for these enzymes. For *Rhodobacter sphaeroides* Cyt*c*O (cytochrome aa_3), it appears as though the E286 side chain of subunit I is a branching point from which protons are shuttled either to the catalytic site for O_2 reduction or to the acceptor site for pumped protons. Amide hydrogen−deuterium exchange mass spectrometry was used to investigate how mutation of this key branching residue to histidine (E286H) affects the structures and dynamics of four redox intermediate states. A functional characterization of this mutant reveals that E286H Cyt*c*O retains ∼1% steady-state activity that is uncoupled from proton pumping and that proton transfer from H286 is significantly slowed. Backbone amide H−D exchange kinetics indicates that specific regions of Cyt*c*O, perturbed by the E286H mutation, are likely to be involved in proton gating and in the exit pathway for pumped protons. The results indicate that redox-dependent conformational changes around E286 are essential for internal proton transfer. E286H Cyt*c*O, however, is incapable of these specific conformational changes and therefore is insensitive to the redox state of the enzyme. These data support a model where the side chain conformation of E286 controls proton translocation in Cyt*c*O through its interactions with the proton gate, which directs the flow of protons either to the active site or to the exit pathway. In the E286H mutant, the proton gate does not function properly and the exit channel is unresponsive. These results provide new insight into the structure and mechanism of proton translocation by Cyt*c*O.

Redox-coupled proton pumps such as cytochrome *c* oxidase (Cyt*c*O)[1] are important enzymes for aerobic energy metabolism (*1*−*3*). Cyt*c*O is a complex, membrane-spanning enzyme that utilizes the free energy released from the reduction of O_2 to transport protons across a membrane. The net result is an electrochemical gradient that is utilized, for example, by ATP synthase to generate the energy source ATP. Four electrons are donated sequentially from cytochrome *c* to the Cyt*c*O dinuclear Cu_A center, from where they are transferred to heme *a*, and further to the binuclear Cu_B/heme a_3 active site where O_2 is reduced to H_2O (Figure 1). This process is coupled to the translocation of eight protons taken from the negative side of the membrane (*4*). Four of these protons are consumed in the reduction of O_2 (substrate protons), and an additional four are pumped across the membrane (pumped protons).

A simplified catalytic reaction scheme for the reduction of O_2 by bacterial Cyt*c*O is shown in Figure 1C. During Cyt*c*O turnover, the oxidized binuclear center (**O**) is reduced with two electrons and two protons to form the reduced state (**R**). When O_2 binds to ferrous heme a_3 (**A**), four electrons and one proton are required to break the O−O bond to form $\mathbf{P_M}$ (*5*, *6*). Three of these electrons are supplied by the binuclear center with an additional electron and proton transferred internally from Y288[2] (*6*). If the initial state of the enzyme is fully reduced (i.e., Cu_A and heme *a* are also reduced), the fourth electron is transferred from heme *a* instead of Y288 to form the $\mathbf{P_R}$ state (*7*). The $\mathbf{P_M}$ and $\mathbf{P_R}$ states are presumably the same, although the $\mathbf{P_R}$ intermediate has an additional electron at the binuclear center (*8*). After formation of $\mathbf{P_M}$, an electron and a proton are transferred, leading to the ferryl intermediate (**F**). The **F** state can also be formed from the $\mathbf{P_R}$ intermediate, but it is only associated

† Supported by Grants R01 GM030910, P30 ES000267, T32 ES007028, and F32 ES013105 from the National Institutes of Health and grants from the Swedish Research Council.

* Author to whom correspondence should be addressed. E-mail: r.armstrong@vanderbilt.edu and peterb@dbb.su.se.

‡ Vanderbilt University.

§ Stockholm University.

Current address: Department of Chemistry, University of Alabama, Tuscaloosa, AL.

[1] Abbreviations used: Cyt*c*O, cytochrome *c* oxidase; **O**, oxidized state; **R**, reduced state; $\mathbf{P_M}$/$\mathbf{P_R}$, "peroxy" state; **F**, "ferryl" state; H-D, hydrogen-deuterium; DDM, n-dodecyl *β*-D-maltoside; HEPES, *N*-(2-hydroxyethyl)piperazine-*N*′-ethanesulfonic acid; PMS, phenazine methosulfate.

[2] Unless otherwise noted, the residue numbers are those for the *Rhodobacter sphaeroides* Cyt*c*O (cytochrome aa_3).

10.1021/bi701643a CCC: $40.75
Published on Web 12/06/2007

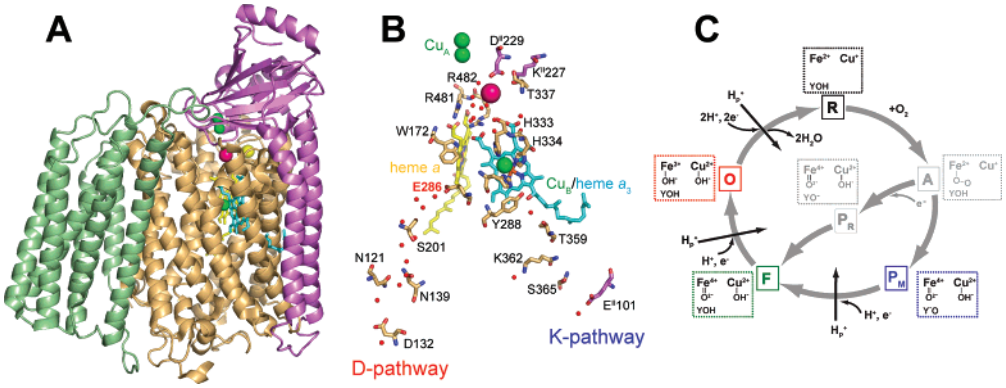

FIGURE 1: *R. sphaeroides* cytochrome *c* oxidase proton-transfer pathways and a simplified reaction scheme. (A) The overall structure of *R. sphaeroides* Cyt*c*O (PDB 1M56) is shown with subunit I in orange, subunit II in purple, and subunit III in green. (B) Residues involved in proton-transfer pathways are shown in stick format, with the D- and K-pathways indicated: Cu_A and Cu_B (green); heme *a* (yellow); heme a_3 (cyan); Mg^{2+} (magenta). The subunit I and II backbone atoms are colored as in panel A. The E286 residue is labeled in red. (C) A simplified version of the reduction of oxygen to water by Cyt*c*O. The oxidized (**O**) catalytic site is reduced to form (**R**). After O_2 binds (**A**), the enzyme forms the "peroxy" intermediate ($\mathbf{P_M}$) with one electron taken presumably from Tyr288 leaving a tyrosyl radical (Y•O). If Cyt*c*O is fully reduced, then the $\mathbf{P_R}$ intermediate is formed where one additional electron (as compared to $\mathbf{P_M}$) is transferred to the catalytic site. The structures of $\mathbf{P_M}$ and $\mathbf{P_R}$ are presumably the same although the $\mathbf{P_R}$ intermediate has an additional electron at the binuclear center. After formation of the **P** intermediate, electron transfer and proton transfer via the D-pathway lead to the **F** intermediate state. Finally, the last electron is transferred to the binuclear center with associated proton uptake through the D-pathway to reform the oxidized protein (**O**). One proton is pumped during both the $\mathbf{P_M}\rightarrow\mathbf{F}$ and $\mathbf{F}\rightarrow\mathbf{O}$ transitions, and possibly two protons for the $\mathbf{O}\rightarrow\mathbf{R}$ transition.

with proton transfer. The **O** state is regenerated with transfer of an additional electron and proton. During enzyme turnover, the $\mathbf{P_{M/R}}\rightarrow\mathbf{F}$, $\mathbf{F}\rightarrow\mathbf{O}$, and possibly $\mathbf{O}\rightarrow\mathbf{R}$ transitions are linked to proton pumping across the membrane (*4*, *9*, *10*). The actual mechanism by which Cyt*c*O and other proton pumps control proton uptake and translocation remains at the forefront of current experimental efforts.

Structural and biochemical analyses of the oxidase enzymes, such as Cyt*c*O from *Rhodobacter sphaeroides*, have identified two spatially distinct proton uptake pathways originating at either the bacterial cell membrane or mitochondrial inner membrane (*11*−*14*). Both the K- and D-pathways contain a series of hydrophilic/polar residues and crystallographically observed water molecules to presumably form hydrogen-bonded chains for proton translocation (Figure 1B). Protons required to reduce the oxidized binuclear center prior to the binding of O_2 are supplied by the K-pathway, which is named for the key residue K362 (*15*, *16*). Alternatively, the D-pathway, which begins at or near D132, is unique in that it provides both substrate and pumped protons (*17*−*19*).

The last identified proton acceptor of the D-pathway is E286. The side chain of E286 or its equivalent in other Cyt*c*O enzymes is a crucial component of this pathway since substitution of this residue by nonprotonatable residues (E286Q) or (E286A) resulted in significantly impaired proton transfer (*18*, *20*−*22*). In the case of the *R. sphaeroides* Cyt*c*O E286Q mutant, the catalytic cycle was blocked after formation of the "peroxy" (**P**) intermediate state, due to impaired proton transfer to the binuclear center via the 286 residue (*18*). Replacement of E286 by the protonatable residue aspartate (E286D) resulted in only a slight decrease in the turnover rate (~50%), and proton pumping was maintained (*23*, *24*).

It is generally agreed that the E286 side chain is a branching point from which protons are shuttled either to the catalytic site or to the acceptor site for pumped protons (reviewed in ref *25*). However, the proton acceptor(s) from E286 for protons to be pumped is unclear. Recent studies indicate that a heme a_3 propionate is one potential acceptor (*26*−*28*). E286 resides in a hydrophobic cavity below hemes *a* and a_3 (Figure 1B), which may contain water molecules. Several theoretical studies indicate that these water molecules could form transient, hydrogen-bonded networks that traverse this cavity and are dependent on the protonation state of E286 (*27*, *29*−*33*). To date, the presence of water chains that connect the E286 side chain to the binuclear center or to the proposed exit pathway have yet to be observed at the molecular level.

It is thought that conformational changes in Cyt*c*O may play a role in regulating proton translocation (*11*, *34*). To address this issue, amide H−D exchange followed by mass spectrometry was previously used to probe structural changes coupled to the redox intermediate states of *R. sphaeroides* Cyt*c*O (Subunits I−III) (*35*). These experiments revealed that backbone amide hydrogens in the vicinity of the hydrophobic cavity rapidly exchanged with deuterium. In order for rapid deuterium exchange to occur, external D_2O (or OD^-) must have access to the interior of the protein (*36*, *37*). This suggests that water molecules in the cavity and those in bulk solution readily equilibrate. In addition, a redox-dependent proton gate that directs the flow of protons was proposed to reside within a section of the protein (residues 169−175) located directly above E286 in the hydrophobic cavity. A section of the putative proton exit channel was also identified through redox-dependent changes in solvent accessibility and protein dynamics. This region, composed of residues 320−340, lies at the subunit I−II interface and contains two histidine ligands to Cu_B. Therefore, this region is a prime candidate for the transmittal of redox-dependent conformational changes that control proton movement through Cyt*c*O.

The aim of the present study is to provide more definitive identification of regions that are linked to proton uptake/transfer through the D-pathway using amide H−D exchange mass spectrometry. To do this, it is important to have a functional, but impaired, mutant enzyme so that the effect

on individual redox intermediate states can be resolved. In this paper we report the effects of the E286H mutation on the activity and structure of Cyt*c*O as assessed by amide H−D exchange mass spectrometry. The E286H mutant of *R. sphaeroides* Cyt*c*O displays approximately 1% steady state activity of the wild-type enzyme, but does not pump protons. The H−D exchange results expose structural perturbations near the site of the mutation that correlate with the severe reduction in steady state activity. It appears that proton uptake/transfer through the D-pathway is linked structurally and functionally to a proposed gating region and exit channel for pumped protons. It is apparent that mutation of E286 perturbs the redox-based linkage and that structural/dynamic changes around E286 are required for proper signaling of proton uptake, gating, and pumping.

EXPERIMENTAL PROCEDURES

Site-Directed Mutagenesis and Purification of E286H CytcO. Site-directed mutagenesis (E286H) of the *R. sphaeroides* cytochrome aa_3 Cyt*c*O was performed as described in ref *16* (see also ref *38*). Bacteria were grown aerobically, and the histidine-tagged enzyme was purified using Ni^{2+}-NTA affinity chromatography, as described in ref *39*.

Activity Measurements of CytcO. The turnover activity of native and E286H Cyt*c*O was determined from the initial oxidation rate of reduced cytochrome *c* (30 μM) upon mixing with the oxidized enzyme (10 nM) in the presence of O_2 in a 50 mM phosphate buffer with 0.1% n-dodecyl β-D-maltoside (DDM) at pH 6.5. Absorbance changes associated with cytochrome *c* oxidation were recorded at 550 nm.

To prepare the fully reduced (with four electrons) Cyt*c*O, frozen stock solutions of Cyt*c*O were solubilized in 0.1% DDM and diluted to a concentration of 10−15 μM in 100 mM HEPES at pH 7.4. The redox mediator phenazine methosulfate (PMS) was added at a concentration of 1 μM. The solution was transferred to an anaerobic cuvette after which the atmosphere was evacuated on a vacuum line and flushed with N_2 several times. In the next step, ascorbate (final concentration 2 mM) was added to the anaerobic Cyt*c*O solution, and the nitrogen was replaced by CO. Formation of the reduced Cyt*c*O−CO complex was confirmed by inspection of the optical absorbance spectrum.

The flow-flash technique was used to investigate the reaction of the reduced Cyt*c*O with O_2 using a modified custom-built combined stopped-flow/flash-photolysis apparatus (LK.60 FF-60, Applied Photophysics Ltd., Surrey, UK) (see ref *15* for a more detailed description). The anaerobic Cyt*c*O−CO complex was mixed with an O_2-saturated solution at a ratio of 1:5 (enzyme:O_2 solution). About 100 ms after mixing, the CO ligand was photodissociated with a 5 ns laser flash (Quantel Brilliant Nd:YAG laser at 532 nm). To monitor the reaction, absorbance changes at single wavelengths were measured with a time resolution of ~1 μs. The amount of reacting enzyme was determined from the CO-dissociation absorbance change at 445 nm.

Proton-Pumping Measurements. CytcO-containing vesicles were prepared as described in Lee et al. (*40*). The vesicle-incorporated enzyme was diluted to 0.5 μM in 50 μM HEPES−KOH, 45 mM KCl, 44 mM sucrose, 1 mM EDTA, 100 μM phenol red at pH 7.5, and the reaction was initiated upon mixing the Cyt*c*O solution with reduced cytochrome *c* (16 μM, in the same solution as above) in a stopped-flow apparatus (Applied Photophysics) at a 1:1 ratio. Proton pumping was measured in the presence of 2 μM valinomycin and proton uptake from the inside of the vesicles in the presence of 2 μM valinomycin and 5 μM FCCP. The absorbance changes of phenol red were recorded at 556.5 nm, which is an isosbestic point for cytochrome *c* oxidation.

Amide Hydrogen−Deuterium Exchange Mass Spectrometry. The mass spectrometry-based sequence identification of peptides generated from a pepsin digest of wild-type Cyt*c*O subunits I−III was reported in Busenlehner et al. (*35*). All peptides identified for wild-type Cyt*c*O were also observed for E286H Cyt*c*O. Additionally, the peptide corresponding to residues 282−292 with the E286H mutation was confirmed by tandem MS−MS sequencing techniques and contains the H284−Y288 covalent cross-link.

The kinetics of H−D exchange of four redox intermediate states of E286H Cyt*c*O (**O**, **R**, $\mathbf{P_M}$, **F**), was followed by electrospray ionization mass spectrometry as previously described (*35*). The oxidized state (**O**) refers to the "as-isolated" protein state. The reduced state (**R**) is the four electron-reduced protein and was formed by incubation with excess sodium dithionite. The $\mathbf{P_M}$ intermediate state was formed by purging anaerobic Cyt*c*O with CO gas prior to exposure to air. The "ferryl" or **F**-intermediate was prepared by adding excess hydrogen peroxide. Formation of each intermediate state was verified by UV−visible spectroscopy as a function of time (data not shown). H−D exchange measurements were recorded within the time regimes indicated by kinetic stabilities of the intermediate states (*35*).

The procedure for hydrogen/deuterium exchange has been described and was followed without exception (*35*). In general, deuterium incorporation was initiated by the addition of D_2O (99.9% at. D) to 110 μM E286H Cyt*c*O. After the appropriate incubation period, in-exchange of deuterium was quenched with aqueous 0.1 M potassium phosphate, pH 2.3. The protein sample was digested with pepsin (5 equiv *w*/*w*) for 8 min on ice then applied to a 1 × 50 mm microbore C18 reversed-phase HPLC column (Phenomenex; Torrence, CA). Peptides were eluted with a linear gradient of increasing acetonitrile, and mass spectra were recorded on a ThermoFinnigan TSQ Quantum triple-quadrupole mass spectrometer using positive ion electrospray ionization. Data were processed using ThermoFinnigan Xcalibur software and MagTran (*41*). The appropriate control samples that correct for loss of deuterium label during HPLC separation ($m_{100\%}$) and for gain of deuterium during protease digestion ($m_{0\%}$) were also included with each data set acquired (*35*, *37*).

The total amount of deuterium incorporated (*D*) as a function of time (*t*) was determined from eq 1, where *N* is the total number of exchangeable amide hydrogens for that peptide, and m_t is the centroid of the isotope envelope at time *t*. Plots of deuterium incorporation as a function of time (average of three independent determinations) were fit either to single-, double-, or triple-exponential equations as indicated by goodness-of-fit values. The amplitudes and rate constants including errors for the fits are given in Tables S1−S6 (Supporting Information) provide an evaluation of the quality of the kinetic data reported.

$$D = N[(m_t - m_{0\%})/(m_{100\%} - m_{0\%})] \qquad (1)$$

RESULTS

Functional Characterization of E286H CytcO. In this report, we investigated the structural and functional effects of altering the local environment within the D-pathway of *R. sphaeroides* Cyt*c*O. For this purpose, the branching point for D-pathway protons, E286, was replaced with the protonatable residue, histidine. A basic functional characterization of the mutant was required prior to structural studies to ensure the enzyme retained activity. The steady-state turnover activity of the mutant Cyt*c*O was determined from the oxidation rate of reduced cytochrome *c* and was found to be ~1% of that of the wild-type enzyme (data not shown). This activity is higher than that of the E286Q mutant investigated previously but significantly lower than that of the E286D mutant, which also carries a protonatable residue at position 286 of subunit I (*18*, *23*, *24*). The optical absorption spectrum for oxidized E286H is essentially the same as that observed with the wild-type Cyt*c*O (data not shown). This indicates that the redox metal centers are not significantly affected by the mutation. Furthermore, the structural integrity of the binuclear center was assessed by measuring the CO-recombination rate after flash-induced dissociation of CO from the fully reduced, anaerobic Cyt*c*O−CO complex. The E286H mutant displays the same rate of recombination as that observed with the wild-type Cyt*c*O (data not shown) (*41*). The E286H mutant, when reconstituted into vesicles, exhibited no significant proton pumping activity in the presence of the ionophore, valinomycin (Figure S1, Supporting Information).

To determine if the E286H mutation influenced internal electron-transfer reactions, we first examined flash-induced electron transfer after dissociation of a CO ligand from the two-electron reduced (mixed-valence) Cyt*c*O in the absence of oxygen (*42*). Laser-flash induced dissociation of CO from reduced heme a_3 leads to a drop in the reduction potential and therefore to rapid internal electron transfer from heme a_3 to heme *a*, and slower transfer from heme *a* to Cu_A. For the E286H mutant, both the rates of electron transfer between heme a_3 and heme *a* and between heme *a* and Cu_A are comparable to wild-type Cyt*c*O (data not shown) (*42*). However, after preparation of the CO-mixed-valence E286H Cyt*c*O a fraction (~50%) of heme *a* is also reduced, which indicates that the midpoint potential of the heme has increased. Similar results have been observed in other experiments where the local environment around E286 has been modified (*43*, *44*).

To investigate the effect of the mutation on internal proton-transfer events, we studied the reaction of the fully reduced, CO-bound Cyt*c*O with O_2 [reviewed in (*25*)]. The rate of binding of O_2 is limited by the off-rate of CO. After rapid photodissociation of the CO ligand, the subsequent binding of O_2 and its stepwise reduction can be followed using time-resolved spectroscopic techniques to provide information about Cyt*c*O intermediate states and the rate of the transitions between them.

With wild-type Cyt*c*O at pH 7.4, four kinetic phases are observed. After an unresolved absorbance change associated with dissociation of the CO ligand (see $t = 0$, Figure 2A), the binding of O_2 results in a decrease in absorbance at 445 nm ($\tau \cong 10$ μs, not resolved on the time scale shown in Figure 2A), followed by a further decrease associated with

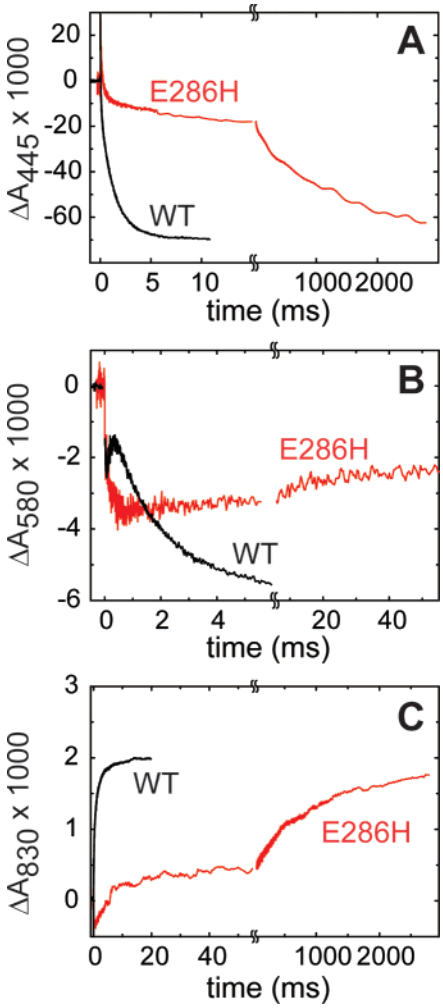

FIGURE 2: Absorbance changes during the reaction of the fully reduced, CO-bound wild-type and E286H Cyt*c*O with O_2. Shown is the stepwise reduction of O_2 after photodissociation of the CO ligand from wild-type (black) and E286H (red) Cyt*c*O. The anaerobic Cyt*c*O−CO complex was mixed with an O_2-saturated solution, and then the CO ligand was photodissociated with a 5 ns laser flash. The reaction was monitored by time-resolved absorbance measurements at (A) 445 nm, (B) 580 nm, and (C) 830 nm. Experimental conditions were 2 μM reacting enzyme (all traces have been normalized to 1 μM reacting enzyme, 0.1 M HEPES buffer, (pH 7.4), 0.1% dodecyl-β-D-maltoside, 1 mM O_2, 22 °C.

formation of the $\mathbf{P_R}$ state with a time constant of ~50 μs, also seen as a decrease in absorbance at 580 nm (Figure 2B). Next, the **F** state is formed with a time constant of ~100 μs, most clearly seen as an absorbance increase at 580 nm (Figure 2B). Concomitantly with the proton uptake upon formation of the **F** state, an electron at Cu_A equilibrates with heme *a*, which results in fractional oxidation of Cu_A and therefore increased absorbance at 830 nm (Figure 2C). Finally, the oxidized Cyt*c*O is formed with a time constant of ~1 ms, observed as a decrease in absorbance at 445 nm (Figure 2A) and an increase in absorbance at 830 nm (Figure 2C) due to oxidation of the remaining fraction of reduced Cu_A.

Flash-induced dissociation of CO from E286H Cyt*c*O results in the binding of O_2 to the reduced catalytic site with the same time constant (~10 μs) as that observed with wild-type Cyt*c*O (Figure 2A). The $\mathbf{P_R}$ state is formed but with a slightly larger time constant ($\tau \sim 80$ μs) and to a lesser extent than with the wild-type Cyt*c*O. The decrease in the formation

of P_R (oxidation of heme *a*) is also consistent with an increase in the midpoint potential of heme *a* (see above). Both the formation of the **F** state and oxidation of Cu_A are slowed by a factor of ~100 to approximately 10 ms in the E286H mutant Cyt*c*O. In addition, formation of the oxidized Cyt*c*O is slowed dramatically and is observed with a main component time constant of ~1.2 s. There is also a small component with a time constant of ~25 ms [*cf.* slow component of the **F→O** transition discussed in (*15*)]. These results demonstrate that the mutant can form the same intermediate states as wild-type Cyt*c*O, but that the rates of the transitions that involve proton transfer from residue 286 are dramatically slowed.

Amide H−D Exchange Mass Spectrometry. Backbone amide H−D exchange mass spectrometry is a structural technique that has been recently applied to membrane-spanning proteins including *R. sphaeroides* Cyt*c*O (*35*, *45*). These kinetic experiments exploit the unique exchange behavior of amide protons in folded proteins (reviewed in ref *37*). Spatial resolution along the backbone is achieved by digestion with pepsin or other acid proteases; therefore, the rate of deuterium incorporation is localized to specific peptide segments of the full-length protein. In general, the amount of deuterium exchanging within 15 s is referred to as the "fast" phase ($k_{ex} > 4$ min^{-1}) and primarily reflects the solvent accessibility of those amide protons to D_2O or OD^-. Amides that exchange in the intermediate time regime are facilitated by dynamic motions that allow for transient exposure of the backbone to deuterium. Thus, amide H−D exchange mass spectrometry supplies information on both structure and dynamics of a protein (*37*).

In general, amide H−D exchange kinetic profiles for subunits II and III in the oxidized (**O**), fully reduced (**R**), "peroxy" ($\mathbf{P_M}$), and ferryl (**F**) intermediate states of the E286H mutant Cyt*c*O are similar to those for the wild-type enzyme published previously (*35*). The only differences in the kinetics of exchange occur for peptides in subunit I, which contains the E286H mutation, heme *a*, and the heme a_3/Cu_B binuclear center. Out of 80 pepsin-generated peptides, only eight display altered deuterium exchange behavior for one or more intermediate states of E286H Cyt*c*O, when compared to wild-type. These peptides are mapped to the structure of subunit I as shown in Figure 3. Three of these peptides (residues 69−72, 78−84, and 254−263), located far from the E286H mutation, show very small differences in exchange compared to wild-type (see Figure S2 and Tables S1 and S2, Supporting Information). The small changes probably do not reflect significant structural perturbations of the protein.

On the other hand, the remaining five peptides with altered backbone H−D exchange kinetics in the mutant are generally located near the site of the mutation (Figure 3). This includes the peptide that contains the E286H mutation (residues 282−292) but also the K-pathway residue Y288 and the Cu_B ligand H284. Mass spectrometry-based sequencing reveals that the Y288−H284 covalent cross-link observed for wild-type Cyt*c*O is indeed present in the mutant (data not shown) (*35*, *46*, *47*).

Overall, amide hydrogens within peptide 282−292 in the four redox states are not very solvent accessible as judged by the very low amplitude of the fast-exchange phase (<15 s) (Figures 4A and 4B). This characteristic is maintained in the mutant Cyt*c*O, as well. The E286H mutation does,

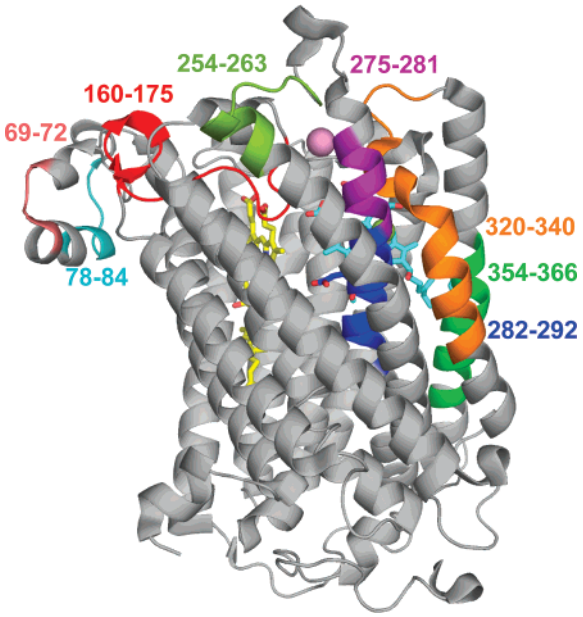

FIGURE 3: Peptides with altered H−D exchange kinetics in E286H Cyt*c*O. Peptides in the E286H mutant that exhibit differences in the rate profiles for deuterium incorporation as compared to wild-type Cyt*c*O and are colored as follows: 69−72 (salmon), 78−84 (teal), 160−175 (red), 254−263 (olive green), 275−281 (purple), 282−292 (blue), 320−340 (orange), and 354−366 (green). Hemes *a* and a_3 are in yellow and cyan, respectively. The site of the E286H mutation is indicated in stick format.

however, influence the deuterium exchange rates for the intermediate time regime. The redox intermediate states affected include the **O**, $\mathbf{P_M}$, and **F** states, which are all characterized by significantly decreased deuterium incorporation compared to wild-type Cyt*c*O (Figures 4A and 4B). This is consistent with a loss of conformational flexibility or dynamics in this region in the E286H mutant. The **R** state does not appear to be influenced by the mutation. These results suggest that the mutation does not affect the solvent accessibility of residues around position 286 but does result in more constrained dynamic motions that might limit transfer of D-pathway protons during the oxidative half of the catalytic cycle. No other peptides that contain residues in the D-pathway exhibit alterations in H−D exchange behavior in the four intermediate states when compared to wild-type Cyt*c*O.

A peptide adjacent to 282−292 is also affected by the mutation of E286 (Figure 3). Peptide 275−281 (^{275}YQHIL-WF^{281}) is a highly hydrophobic peptide with an α-helical conformation that has multiple hydrogen-bonding interactions to residues in peptides around the active site (320−340, 282−292, and 160−175). Most amides within peptide 275−281 of the wild-type enzyme exhibit restricted solvent access in all of the intermediate states (Figure 4C) (*35*). However, it is clear that this region undergoes redox-dependent, dynamic fluctuations based on the distribution of intermediate time regime exchange rates (i.e., **O** exchanges faster than **R**). However in the mutant, all redox states have similar rate profiles (Figure 4D). This clearly suggests that redox-specific changes in conformational dynamics observed with wild-type Cyt*c*O are more restricted in the E286H mutant. These data are consistent with results obtained for residues 282−292, which also show decreased dynamics in the mutant Cyt*c*O.

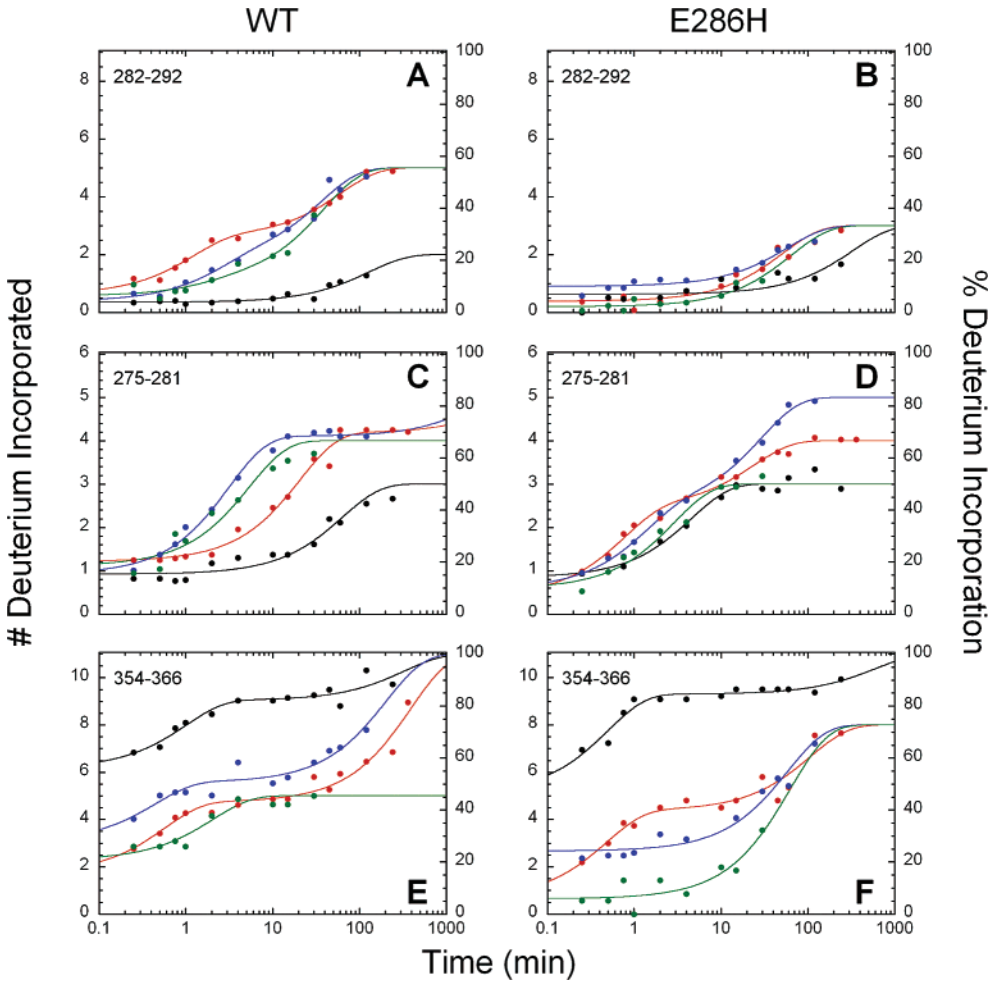

FIGURE 4: Kinetic profiles for key peptides exhibiting changes in H−D exchange in the E286H mutant. The kinetic traces for three peptides of subunit I are shown: residues 282−292 (panels A and B), 275−281 (panels C and D), and 354−366 (panels E and F). The total number (left axis) and the percentage (right axis) of deuterium incorporated are plotted as a function of time. The solid lines indicate single- or double-exponential fits to the data with the amplitudes, rate constants, and errors for the fits given in Tables S3 and S4 (Supporting Information). Each redox intermediate state is represented by a separate trace: **O** (red), **R** (black), $\mathbf{P_M}$ (blue), **F** (green). Wild-type Cyt*c*O H−D exchange kinetic traces (left column) have been published previously (*35*) and are shown for purposes of comparison to those of E286H Cyt*c*O (right column).

Peptide 354−366, which contains three residues involved in proton translocation through the K-pathway, is also affected by the E286H mutation (Figures 4E and 4F). For wild-type Cyt*c*O (Figure 4E), peptide 354−366 undergoes a specific conformational change in the **R** state that increases the solvent accessibility of amides in the K-pathway. The increase in deuterium incorporation has been interpreted to be due to opening of the K-pathway (*35*), allowing water to participate in proton translocation in the reductive half of the cycle (**O**→**R**). The kinetic profiles for H−D exchange in the **O** and **R** states of E286H Cyt*c*O are essentially the same as those observed in the wild-type enzyme (Figure 4E and 4F). In contrast, the $\mathbf{P_M}$ and **F** intermediate states have clearly altered kinetic profiles. It appears that backbone amide groups in the K-pathway have more restricted access to solvent in these redox states.

Previous H−D exchange experiments indicated that the loop containing W172 (residues 160−175) may be a significant region for Cyt*c*O proton gating (*35*). Residues 160−175 form a loop directly above E286 (Figure 3) and reside in a hydrophobic yet solvent accessible region of the protein as shown by the high level of deuterium incorporation in the fast phase (<15 s) for the **O**, **R**, and $\mathbf{P_M}$ intermediates (Figure 5A). The **F** intermediate for 160−175 is unique in that it displays a considerable decrease in H_2O/D_2O access concomitant with an *increase* in deuterium exchange for residues 320−340 in the putative exit channel (Figure 5C). Taken together, the H−D exchange results indicate that the 160−175 loop could act as a proton/water gate between E286 and the exit pathway in the wild-type enzyme (see refs *35* and *48* for a more detailed discussion). The only peptide in the **F** intermediate that is clearly affected by the E286 mutation is peptide 160−175 (Figure 5B). Basically, the mutant enzyme does not change conformation or solvent accessibility in the **F** intermediate as was observed in the wild-type enzyme. Inasmuch as proton pumping occurs both before and after formation of the **F** state ($\mathbf{P_M}$→**F** and **F**→**O**), this "trapped" intermediate represents a specific conformation of Cyt*c*O that is poised for subsequent proton translocation reactions. This conformational state is altered in E286H Cyt*c*O and may correlate with the striking decrease in proton-transfer rates exhibited by the mutant.

The H−D exchange behavior of peptide 160−175 (the proton gate) is coupled to residues 320−340 in wild-type Cyt*c*O (*35*). As shown in Figure 3, peptide 320−340 is part of an unusual, distorted transmembrane α-helix containing

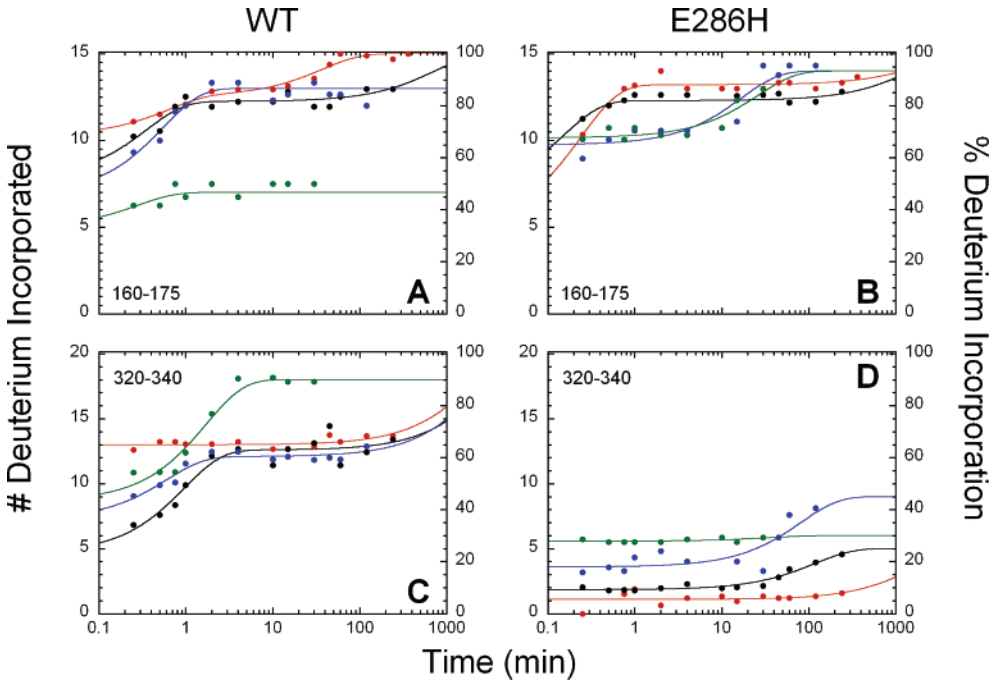

FIGURE 5: Gating and putative proton exit regions display changes in H−D exchange kinetics for E286H Cyt*c*O. The kinetic traces for two peptides of subunit I are shown: residues 160−175 (panels A and B) and 320−340 (panels C and D). The total number (left axis) or the percentage (right axis) of deuterium incorporated are plotted as a function of time. The solid lines indicate single- or double-exponential fits to the data with the amplitudes, rate constants, and errors for the fits given in Tables S5 and S6 (Supporting Information). Each redox intermediate state is represented by a separate trace: **O** (red), **R** (black), $\mathbf{P_M}$ (blue), **F** (green). Wild-type Cyt*c*O H−D exchange kinetic traces (left column) have been published previously (*35*) and are shown for purposes of comparison to those of E286H Cyt*c*O (right column).

two histidine ligands to Cu_B (Figure 1B). A portion of this peptide lines a water channel that has been implicated in the proton exit route (*31*, *49*). In the wild-type Cyt*c*O, residues 320−340 are generally accessible to deuterium in all intermediate states. The **F** state, however, specifically shows enhanced deuterium incorporation over the full time course (Figure 5C). Unlike wild-type Cyt*c*O, the E286H mutant exhibits a large decrease in the level of deuterium label for *all* intermediate states compared to their wild-type counterparts (Figure 5D). For example, the amount of deuterium incorporated in the fast phase (i.e., by 15 s) for the oxidized enzymes decreases from 65% for wild-type to 5% for E286H Cyt*c*O. In other words, these amide protons are more protected from solvent in the mutant compared to wild-type, demonstrating a significant change in conformation or environment. Given that two of the Cu_B ligands are located within this stretch of backbone, it is important to note that the metal centers at the active site do not appear to be perturbed based on the absorption spectrum of the mutant.

DISCUSSION

E286H Mutation Results in Altered Proton Transfer. We have investigated the catalytic and structural effects resulting from mutation of a key residue in proton uptake and transfer within the D-pathway, E286. In general, mutation of E286 results in perturbed proton delivery to the catalytic site and the output side, while some mutations completely impair function (e.g. E286Q) (*18*, *20*−22). The mutation chosen for this work, E286H, is still capable of side chain protonation and does not appear to disturb the environment around the redox metal centers in Cyt*c*O. However, the steady state activity of E286H Cyt*c*O is significantly lowered (1% of the wild-type enzyme) and is no longer coupled to proton pumping.

The E286H mutant enzyme is capable of forming each redox intermediate state as followed by flow-flash techniques with O_2 (Figure 2) and can be fully oxidized. The time constants for the preliminary steps in the reaction cycle ($\mathbf{R}\rightarrow\mathbf{A}\rightarrow\mathbf{P_R}$) are similar to those for the wild-type enzyme. However, the rates of the $\mathbf{P_R}\rightarrow\mathbf{F}$ and $\mathbf{F}\rightarrow\mathbf{O}$ transitions are reduced in the mutant 100- and 1000-fold, respectively. Results from earlier studies have shown that formation of the **F** state is linked to proton uptake through the D-pathway, which also determines the rate of the $\mathbf{P_R}\rightarrow\mathbf{F}$ transition. The proton-transfer takes place in two steps: the proton needed for formation of the **F** state is first taken internally from E286 and transferred to the binuclear center, followed by reprotonation via the D-pathway (*50*, *51*). Because formation of the **F** state is slowed in the E286H mutant Cyt*c*O, the results indicate that proton transfer from H286 to the catalytic site is affected. The $\mathbf{F}\rightarrow\mathbf{O}$ transition also involves proton uptake through the D-pathway. In this case, however, the rate of uptake is also determined by internal electron transfer to the catalytic site (*28*). Thus, the dramatically slowed $\mathbf{F}\rightarrow\mathbf{O}$ transition for E286H Cyt*c*O is consistent with slowed proton transfer since electron-transfer events do not seem to be perturbed in the mutant. Given that the E286H mutant does not pump protons (Figure S1, Supporting Information), the protons provided by the D-pathway must be used as substrate protons for the reduction of O_2 to H_2O.

The orientation and hydrogen-bonding of the E286 carboxylate side chain has been proposed to be involved in determining the rate of proton-transfer events (*52*), which presumably could also affect the rates of the $\mathbf{P}\rightarrow\mathbf{F}$ and $\mathbf{F}\rightarrow\mathbf{O}$

transitions. Given the significant reduction in the time constants for these transitions in the E286H mutant and the lack of proton pumping, the histidine mutation is obviously deleterious to proton transfer. Mutation of E286 to another protonatable side chain, namely the more conservative E286D mutation, does not inhibit Cyt*c*O proton-transfer events to the same extent as in E286H. In fact, the rates of the $\mathbf{P_R}\rightarrow\mathbf{F}$ and $\mathbf{F}\rightarrow\mathbf{O}$ transitions for E286D Cyt*c*O are only decreased 5-fold and 1.5-fold, respectively (*23*). Inasmuch as proton-transfer events that may be linked to structural changes around residue 286 are altered, E286H Cyt*c*O is a prime candidate for structural studies using backbone amide hydrogen−deuterium exchange mass spectrometry.

E286H Affects the Connectivity between E286 and the Binuclear Center. Previous amide H−D exchange experiments with wild-type Cyt*c*O indicated that water molecules in the D-pathway may form a kinetically stable, hydrogen-bonded proton conducting "wire" (*35*). The conformation of several D-pathway spanning peptides were clearly not affected by the redox-state, with the exception of peptide 282−292 (Figure 4A) (*35*). This was not entirely unexpected since several lines of evidence indicate that E286 alters its conformation with the redox state of the enzyme, thus controlling proton transfer (*27*, *29*, *30*, *32*). Yet, it is still unclear what structural changes are required for proton transfer from E286. Identification of regions that may be functionally or structurally interacting with the region around E286 (peptide 282−292) may provide some clues into this process.

The results from amide H−D exchange experiments with the E286H mutant reveal that for all intermediate states, the 282−292 peptide is now more dynamically constrained (i.e., slower rates of deuterium incorporation) than the corresponding peptide from the wild-type enzyme (Figure 4A and 4B). The H−D exchange results with peptide 275−281 indicate that the restriction of backbone dynamics in the mutant extends beyond residues 282−292 to an adjacent peptide segment (Figure 4C and 4D). The diminished dynamic motions deduced in the E286H mutant may signify that the larger side chain of histidine compared to glutamate might prevent H286 from changing its conformation during turnover or that additional hydrogen bonds have been established. Regardless, the region around the E286H mutation does not change conformation in response to the redox state of the binuclear center, a result that suggests E286H Cyt*c*O cannot "sense" the redox state of the enzyme to the same extent as the native enzyme. One explanation of this behavior is that a structural connectivity to the Cu_B/heme a_3 binuclear center has been disrupted by mutation of E286. This disruption may partially account for the decreased time constants for steps requiring proton transfer from residue 286 ($\mathbf{P_M}\rightarrow\mathbf{F}$ and $\mathbf{F}\rightarrow\mathbf{O}$).

Proton Gate and Exit Channel Conformations are Functionally and Structurally Linked. Comparison of the H−D exchange behavior of E286H and wild-type Cyt*c*O also reveals possible connections between the region around E286 and other areas likely to be involved in proton pumping (*35*). These data support the hypothesis that the orientation of the E286 side chain may be intimately coupled to opening and closing of the proton exit channel (*9*, *53*). The H−D exchange results presented here and in an earlier study indicate that the proposed gating region (residues 160−175) may modulate these conformational changes (*35*). Unfortunately, the crystallographic structures have not confirmed such behavior, but one must consider that these structures only provide a static view of Cyt*c*O. The H−D exchange kinetic results report on the structure of Cyt*c*O in solution as a function of redox state, which is missing in the X-ray crystallographic analysis of the enzyme structure.

From an earlier study with native Cyt*c*O (also shown in Figure 5A and 5C), we found that the **F** intermediate conformational state is characterized by decreased solvent accessibility for the proposed gating region (160−175), which is associated with opening of the proton exit channel (320−340) (*35*). Unlike the wild-type Cyt*c*O, the 160−175 peptide of E286H Cyt*c*O does not exhibit decreased deuterium incorporation in the **F** intermediate but instead remains in its solvent accessible conformation (Figure 5B). In terms of structure, the trapped **F** intermediate state may be unique in that proton pumping occurs before and after its formation (Figure 1C); therefore, this enzyme conformation is likely optimized for efficient D-pathway proton uptake and transfer. In this state, the exit channel is water-accessible and the D-pathway is primed for proton uptake (*35*). Functionally, the 160−175 gate is proposed to prevent a "short-circuit" by blocking water/proton connectivity across the membrane.

The results shown in Figure 5 indicate that with the E286H mutant, the 160−175 gate is not functioning properly since it remains solvent-accessible in the **F** intermediate state. As a consequence, the exit channel as defined by residues 320−340 fails to open appropriately and remains virtually closed to water in all redox intermediate states (Figure 5D). This result is very much different from that observed for the wild-type enzyme (*35*). The perturbation to the H−D exchange behavior of residues 320−340 by the E286H mutation is striking. The reason why this region is highly and specifically affected by the mutation of E286 is unknown but can best be described by a model where the side chain of E286 and the exit channel are connected through space, possibly via a hydrogen-bonding network. H−D exchange mass spectrometry provides evidence that structural/dynamic changes around E286 are required for proper signaling of proton uptake, gating, and pumping. In other words, the mutation is not simply influencing the rate of proton transfer from H286 but also a specific Cyt*c*O "proton transfer" conformation that is linked to the redox state of the enzyme. These results are important to understanding Cyt*c*O function because crystallography has yet to reveal significant redox-dependent conformational changes.

Potential Conduit for Proton Exit. The question as to how E286 is connected to the exit pathway for pumped protons remains to be answered. The crystal structures of the wild-type and the E286Q Cyt*c*O enzymes are useful in this regard. In the wild-type structure (Figure 6), the side chain of E286 is hydrogen-bonded to the carbonyl oxygen of M107 (*11*). Based on the E286Q Cyt*c*O structure, when E286 is deprotonated (simulated by the E286Q mutation), this hydrogen bond is broken. In addition, both a postulated gating residue W172 and a heme a_3 propionate change conformation along with a reallocation of waters in the hydrophobic cavity. This presumably connects E286 to the pumping element through a hydrogen-bonded water chain (*11*). The highly conserved residue W172 (located in peptide 160−175) is also in van der Waals contact with M107.

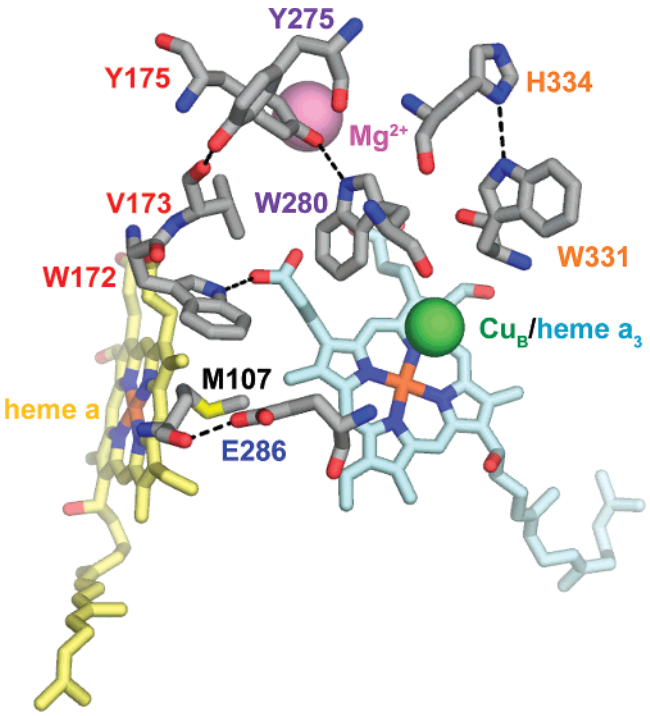

FIGURE 6: Potential interactions linking proton uptake, gating, and exit pathways. Several potential hydrogen-bonding interactions (dashed lines) are indicated on the structure of subunit I of wild-type *R. sphaeroides* Cyt*c*O. Specific residues from peptides exhibiting changes in amide H−D exchange kinetics are shown in stick format along with the hydrogen-bonding partners and are color-coded as in Figure 3: 160−175 (red), 275−281 (purple), 282−292 (blue), and 320−340 (orange). Other potential hydrogen bonds in these regions were observed but were omitted for clarity. In addition, there are several hydrophobic interactions connecting these regions, as well.

Therefore, changes in the orientation of the side chain of E286 can affect hydrogen bonding with M107, and further to W172 in the gating region. W172 is hydrogen-bonded to the heme a_3 Δ-propionate that is thought to be involved in the exit route for pumped protons (*26*−*28*, *48*). The inability of peptide 160−175 to respond to the redox state in the mutant Cyt*c*O correlates with the inability of E286H Cyt*c*O to pump protons. On the basis of the structure of Cyt*c*O, it seems likely that W172 could be involved in gating protons in the wild-type enzyme through redox-associated conformational changes.

Several residues line a hydrophobic tunnel formed by residues W172, V173, L174, P176, L279, W280, F282, and G283 in wild-type Cyt*c*O. Molecular dynamics simulations have indicated that this conduit may provide linkage between E286 and the Δ-propionate of heme a_3 through water chain formation from W172 to W280 (*27*). The amide H−D exchange behavior of E286H Cyt*c*O identifies peptides lining this conduit (160−175, 275−281, 282−292) through altered deuterium incorporation kinetics. The E286H mutation clearly perturbs the structure and dynamics of this channel. As a result, the conduit may not support the water chain formation that would allow for proton pumping across the membrane. Again, gating residues 160−175 may be involved in organizing the appropriate pumping conformation.

Implications for the Mechanism of Proton Gating. It is interesting to note that the E286H mutation is located below the hemes, yet most of the conformational differences between wild-type and mutant Cyt*c*O are localized above the hemes with no spectroscopic indication of any perturbations of the redox centers. Therefore, it appears that solvent access to residues on the output side (exit channel) is altered even though the blockage is on the input side (E286H). This observation would suggest that solvent access to the output side is "controlled" by a region of the protein located at or below the hemes and may involve hydrogen-bonding interactions mediated by the configuration of the 160−175 gating loop. Functional work on the W164F mutant of *P. denitrificans* Cyt*c*O (W172F in *R. sphaeroides*) provides support for its involvement in proton-transfer reactions due to the reduced steady state activity (40% of wild-type) and decreased proton pumping efficiency (*43*). Moreover, the time constants for the $\mathbf{P_R}\rightarrow\mathbf{F}$ and $\mathbf{F}\rightarrow\mathbf{O}$ transitions are significantly lowered to values similar to those for *R. sphaeroides* E286H Cyt*c*O. The authors conclude that the W172F mutation probably affects the side chain orientation of E286. This constitutes another line of evidence that the structure of the gating loop, particularly W172, is connected to the structure/dynamics of the branching residue E286, which are both dependent on the redox state of the enzyme.

Conclusions. The amide H−D exchange mass spectrometry experiments presented here highlight some of the structural requirements for proton uptake, gating, and pumping in *R. sphaeroides* Cyt*c*O. We propose that redox-dependent conformational changes around E286 are critical for directing proton transfer through interaction(s) with the gating loop (residues 160−175). The conformation of the gating loop is also linked to the opening and closing of the proton exit channel (residues 320−340). Here, we show that the linkage is broken (uncoupled) by replacement of E286, which is a central element in controlling transfer of pumped protons. These results are consistent with a functional model where deprotonation of E286 is linked to a structural change, which provides access to the proton exit pathway. Such structural changes likely control proton transfer across the membrane. It is interesting to note that residues within the regions affected by the E286H mutation are well conserved in various cytochrome *c* oxidases. Therefore, the mechanistic insight provided here through amide H−D exchange mass spectrometry should be applicable to other oxidase enzymes.

SUPPORTING INFORMATION AVAILABLE

Figure S1 illustrating the lack of proton pumping by E286H, Figure S2 and Tables S1 and S2 comparing the kinetic profiles, amplitudes, and rate constants for H−D exchange in peptides 69−72, 78−84, and 254−263 for the wild-type and the E286H mutant CytcO in all four intermediate states and Tables S3−S6 comparing the amplitudes and rate constants for H−D exchange in peptides 160−175, 275−281, 282−292, 320−340, 354−366 for the wild-type and E286H mutant CytcO in all four intermediate states. This material is available free of charge via the Internet at http://pubs.acs.org.

REFERENCES

1. Hosler, J. P., Ferguson-Miller, S., and Mills, D. A. (2006) Energy transduction: proton transfer through the respiratory complexes, *Annu. Rev. Biochem. 75*, 165−187.
2. Gennis, R. B. (2004) Coupled proton and electron transfer reactions in cytochrome oxidase, *Front. Biosci. 9*, 581−591.

3. Brzezinski, P. (2004) Redox-driven membrane-bound proton pumps, *Trends Biochem. Sci. 29*, 380−387.
4. Wikström, M. (1989) Identification of the electron transfers in cytochrome oxidase that are coupled to proton-pumping, *Nature 338*, 776−778.
5. Iwaki, M., Puustinen, A., Wikström, M., and Rich, P. R. (2003) ATR-FTIR spectroscopy of the P_M and F intermediates of bovine and *Paracoccus denitrificans* cytochrome *c* oxidase, *Biochemistry 42*, 8809−8817.
6. Proshlyakov, D. A., Pressler, M. A., DeMaso, C., Leykam, J. F., DeWitt, D. L., and Babcock, G. T. (2000) Oxygen activation and reduction in respiration: involvement of redox-active tyrosine 244, *Science 290*, 1588−1591.
7. Ädelroth, P., Ek, M., and Brzezinski, P. (1998) Factors determining electron-transfer rates in cytochrome *c* oxidase: investigation of the oxygen reaction in the *R. sphaeroides* enzyme, *Biochim. Biophys. Acta 1367*, 107−117.
8. Morgan, J. E., Verkhovsky, M. I., and Wikström, M. (1996) Observation and assignment of peroxy and ferryl intermediates in the reduction of dioxygen to water by cytochrome *c* oxidase, *Biochemistry 35*, 12235−12240.
9. Faxén, K., Gilderson, G., Ädelroth, P., and Brzezinski, P. (2005) A mechanistic principle for proton pumping by cytochrome *c* oxidase, *Nature 437*, 286−289.
10. Bloch, D., Belevich, I., Jasaitis, A., Ribacka, C., Puustinen, A., Verkhovsky, M. I., and Wikström, M. (2004) The catalytic cycle of cytochrome *c* oxidase is not the sum of its two halves, *Proc. Natl. Acad. Sci. U.S.A. 101*, 529−533.
11. Svensson-Ek, M., Abramson, J., Larsson, G., Törnroth, S., Brzezinski, P., and Iwata, S. (2002) The X-ray crystal structures of wild-type and EQ(I-286) mutant cytochrome *c* oxidases from *Rhodobacter sphaeroides*, *J. Mol. Biol. 321*, 329−339.
12. Iwata, S., Ostermeier, C., Ludwig, B., and Michel, H. (1995) Structure at 2.8 Å resolution of cytochrome *c* oxidase from *Paracoccus denitrificans*, *Nature 376*, 660−669.
13. Tsukihara, T., Aoyama, H., Yamashita, E., Tomizaki, T., Yamaguchi, H., Shinzawa-Itoh, K., Nakashima, R., Yaono, R., and Yoshikawa, S. (1996) The whole structure of the 13-subunit oxidized cytochrome c oxidase at 2.8 Å, *Science 272*, 1136−1144.
14. Wikström, M., Jasaitis, A., Backgren, C., Puustinen, A., and Verkhovsky, M. I. (2000) The role of the D- and K-pathways of proton transfer in the function of the haem-copper oxidases, *Biochim. Biophys. Acta 1459*, 514−520.
15. Brändén, M., Sigurdson, H., Namslauer, A., Gennis, R. B., Ädelroth, P., and Brzezinski, P. (2001) On the role of the K-proton transfer pathway in cytochrome *c* oxidase. *Proc. Natl. Acad. Sci. U.S.A. 98*, 5013−5018.
16. Hosler, J. P., Shapleigh, J. P., Mitchell, D. M., Kim, Y., Pressler, M. A., Georgiou, C., Babcock, G. T., Alben, J. O., Ferguson-Miller, S., and Gennis, R. B. (1996) Polar residues in helix VIII of subunit I of cytochrome *c* oxidase influence the activity and the structure of the active site, *Biochemistry 35*, 10776−10783.
17. Hosler, J. P., Ferguson-Miller, S., Calhoun, M. W., Thomas, J. W., Hill, J., Lemieux, L., Ma, J., Georgiou, C., Fetter, J., Shapleigh, J., and et al. (1993) Insight into the active-site structure and function of cytochrome oxidase by analysis of site-directed mutants of bacterial cytochrome aa_3 and cytochrome *bo*, *J. Bioenerg. Biomembr. 25*, 121−136.
18. Ädelroth, P., Ek, M. S., Mitchell, D. M., Gennis, R. B., and Brzezinski, P. (1997) Glutamate 286 in cytochrome aa_3 from *Rhodobacter sphaeroides* is involved in proton uptake during the reaction of the fully-reduced enzyme with dioxygen, *Biochemistry 36*, 13824−13829.
19. Konstantinov, A. A., Siletsky, S., Mitchell, D., Kaulen, A., and Gennis, R. B. (1997) The roles of the two proton input channels in cytochrome *c* oxidase from *Rhodobacter sphaeroides* probed by the effects of site-directed mutations on time-resolved electrogenic intraprotein proton transfer, *Proc. Natl. Acad. Sci. U.S.A. 94*, 9085−9090.
20. Verkhovskaya, M. L., García-Horsman, A., Puustinen, A., Rigaud, J. L., Morgan, J. E., Verkhovsky, M. I., and Wikström, M. (1997) Glutamic acid 286 in subunit I of cytochrome bo_3 is involved in proton translocation, *Proc. Natl. Acad. Sci. U.S.A. 94*, 10128−10131.
21. Tsubaki, M., Hori, H., and Mogi, T. (1997) Glutamate-286 mutants of cytochrome *bo*-type ubiquinol oxidase from *Escherichia coli*: influence of mutations on the binuclear center structure revealed by FT-IR and EPR spectroscopies, *FEBS Lett. 416*, 247−250.
22. Svensson-Ek, M., Thomas, J. W., Gennis, R. B., Nilsson, T., and Brzezinski, P. (1996) Kinetics of electron and proton transfer during the reaction of wild type and helix VI mutants of cytochrome bo_3 with oxygen, *Biochemistry 35*, 13673−13680.
23. Ädelroth, P., Karpefors, M., Gilderson, G., Tomson, F. L., Gennis, R. B., and Brzezinski, P. (2000) Proton transfer from glutamate 286 determines the transition rates between oxygen intermediates in cytochrome *c* oxidase, *Biochim. Biophys. Acta 1459*, 533−539.
24. Jünemann, S., Meunier, B., Fisher, N., and Rich, P. R. (1999) Effects of mutation of the conserved glutamic acid-286 in subunit I of cytochrome *c* oxidase from *Rhodobacter sphaeroides*, *Biochemistry 38*, 5248−5255.
25. Brändén, G., Gennis, R. B., and Brzezinski, P. (2006) Transmembrane proton translocation by cytochrome *c* oxidase, *Biochim. Biophys. Acta 1757*, 1052−1063.
26. Puustinen, A., and Wikström, M. (1999) Proton exit from the heme-copper oxidase of *Escherichia coli*, *Proc. Natl. Acad. Sci. U.S.A. 96*, 35−37.
27. Seibold, S. A., Mills, D. A., Ferguson-Miller, S., and Cukier, R. I. (2005) Water Chain Formation and Possible Proton Pumping Routes in *Rhodobacter sphaeroides* Cytochrome *c* Oxidase: A Molecular Dynamics Comparison of the Wild Type and R481K Mutant, *Biochemistry 44*, 10475−10485.
28. Brändén, G., Brändén, M., Schmidt, B., Mills, D. A., Ferguson-Miller, S., and Brzezinski, P. (2005) The protonation state of a heme propionate controls electron transfer in cytochrome *c* oxidase, *Biochemistry 44*, 10466−10474.
29. Riistama, S., Hummer, G., Puustinen, A., Dyer, R. B., Woodruff, W. H., and Wikström, M. (1997) Bound water in the proton translocation mechanism of the haem-copper oxidases, *FEBS Lett. 414*, 275−280.
30. Zheng, X., Medvedev, D. M., Swanson, J., and Stuchebrukhov, A. A. (2003) Computer simulation of water in cytochrome *c* oxidase, *Biochim. Biophys. Acta 1557*, 99−107.
31. Wikström, M., Verkhovsky, M. I., and Hummer, G. (2003) Water-gated mechanism of proton translocation by cytochrome *c* oxidase, *Biochim. Biophys. Acta 1604*, 61−65.
32. Cukier, R. I. (2004) Quantum molecular dynamics simulation of proton transfer in cytochrome *c* oxidase, *Biochim. Biophys. Acta 1656*, 189−202.
33. Tashiro, M., and Stuchebrukhov, A. A. (2005) Thermodynamic properties of internal water molecules in the hydrophobic cavity around the catalytic center of cytochrome *c* oxidase, *J. Phys. Chem. B 109*, 1015−1022.
34. Mills, D. A., and Ferguson-Miller, S. (2003) Understanding the mechanism of proton movement linked to oxygen reduction in cytochrome *c* oxidase: lessons from other proteins. *FEBS Lett. 545*, 47−51.
35. Busenlehner, L. S., Salomonsson, L., Brzezinski, P., and Armstrong, R. N. (2006) Mapping protein dynamics in catalytic intermediates of the redox-driven proton pump cytochrome *c* oxidase. *Proc. Natl. Acad. Sci. U.S.A. 103*, 15398−15403.
36. Smith, D. L., Deng, Y., and Zhang, Z. (1997) Probing the non-covalent structure of proteins by amide hydrogen exchange and mass spectrometry, *J. Mass. Spectrom. 32*, 135−146.
37. Busenlehner, L. S., and Armstrong, R. N. (2005) Insights into enzyme structure and dynamics elucidated by amide H/D exchange mass spectrometry, *Arch. Biochem. Biophys. 433*, 34−46.
38. Aagaard, A., Gilderson, G., Mills, D. A., Ferguson-Miller, S., and Brzezinski, P. (2000) Redesign of the proton-pumping machinery of cytochrome *c* oxidase: proton pumping does not require Glu-(I-286), *Biochemistry 39*, 15847−15850.
39. Mitchell, D. M., and Gennis, R. B. (1995) Rapid purification of wildtype and mutant cytochrome *c* oxidase from *Rhodobacter sphaeroides* by $Ni^{(2+)}$-NTA affinity chromatography, *FEBS Lett. 368*, 148−150.
40. Lee, H. M., Das, T. K., Rousseau, D. L., Mills, D., Ferguson-Miller, S., and Gennis, R. B. (2000) Mutations in the Putative H-Channel in the Cytochrome *c* Oxidase from *Rhodobacter sphaeroides* Show That This Channel Is Not Important for Proton Conduction but Reveal Modulation of the Properties of Heme *a*, *Biochemistry 39*, 2989−2996.
41. Zhang, Z., and Marshall, A. G. (1998) A universal algorithm for fast and automated charge state deconvolution of electrospray mass-to-charge ratio spectra. *J. Am. Soc. Mass Spectrom. 9*, 225−233.

42. Ädelroth, P., Brzezinski, P., and Malmström, B. G. (1995) Internal electron transfer in cytochrome *c* oxidase from *Rhodobacter sphaeroides*, *Biochemistry 34*, 2844−2849.
43. Ribacka, C., Verkhovsky, M. I., Belevich, I., Bloch, D. A., Puustinen, A., and Wikström, M. (2005) An Elementary Reaction Step of the Proton Pump Is Revealed by Mutation of Tryptophan-164 to Phenylalanine in Cytochrome *c* Oxidase from *Paracoccus denitrificans*, *Biochemistry 44*, 16502−16512.
44. Namslauer, A., Lepp, H., Brändén, M., Jasaitis, A., Verkhovsky, M. I., and Brzezinski, P. (2007) Plasticity of proton pathway structure and water coordination in cytochrome *c* oxidase, *J. Biol. Chem. 282*, 15148−15158.
45. Busenlehner, L. S., Codreanu, S. G., Holm, P. J., Bhakat, P., Hebert, H., Morgenstern, R., and Armstrong, R. N. (2004) Stress sensor triggers conformational response of the integral membrane protein MGST1, *Biochemistry 43*, 11145−11152.
46. Qin, L., Hiser, C., Mulichak, A., Garavito, R. M., and Ferguson-Miller, S. (2006) Identification of conserved lipid/detergent-binding sites in a high-resolution structure of the membrane protein cytochrome *c* oxidase, *Proc. Natl. Acad. Sci. U.S.A. 103*, 16117−16122.
47. Rauhamaki, V., Baumann, M., Soliymani, R., Puustinen, A., and Wikström, M. (2006) Identification of a histidine-tyrosine cross-link in the active site of the cbb_3-type cytochrome *c* oxidase from *Rhodobacter sphaeroides*, *Proc. Natl. Acad. Sci. U.S.A. 103*, 16135−16140.
48. Wikström, M., Ribacka, C., Molin, M., Laakkonen, L., Verkhovsky, M., and Puustinen, A. (2005) Gating of proton and water transfer in the respiratory enzyme cytochrome *c* oxidase, *Proc. Natl. Acad. Sci. U.S.A. 102*, 10478−10481.
49. Popović, D. M., and Stuchebrukhov, A. A. (2005) Proton Exit Channels in Bovine Cytochrome *c* Oxidase, *J. Phys. Chem. B 109*, 1999−2006.
50. Namslauer, A., Aagaard, A., Katsonouri, A., and Brzezinski, P. (2003) Intramolecular proton-transfer reactions in a membrane-bound proton pump: the effect of pH on the peroxy to ferryl transition in cytochrome *c* oxidase, *Biochemistry 42*, 1488−1498.
51. Smirnova, I. A., Ädelroth, P., Gennis, R. B., and Brzezinski, P. (1999) Aspartate-132 in cytochrome *c* oxidase from *Rhodobacter sphaeroides* is involved in a two-step proton transfer during oxo-ferryl formation, *Biochemistry 38*, 6826−6833.
52. Pomes, R., and Roux, B. (1998) Free energy profiles for H^+ conduction along hydrogen-bonded chains of water molecules, *Biophys. J. 75*, 33−40.
53. Brzezinski, P., and Larsson, G. (2003) Redox-driven proton pumping by heme-copper oxidases, *Biochim. Biophys. Acta 1605*, 1−13.

BI701643A